Materials and Design 59 (2014) 50–62

Contents lists available at ScienceDirect

Materials and Design

journal homepage: www.elsevier.com/locate/matdes

Analysis of process parameters effects on friction stir welding of dissimilar aluminum alloy to advanced high strength steel

Xun Liu, Shuhuai Lan, Jun Ni *

S.M. Wu Manufacturing Research Center, Department of Mechanical Engineering, University of Michigan, Ann Arbor, MI 48109, USA

ARTICLE INFO

Article history:
Received 22 October 2013
Accepted 1 February 2014
Available online 7 February 2014

Keywords:
Friction stir welding
Dissimilar aluminum/high strength steel
Process parameters
Intermetallic compound
Tensile strength

ABSTRACT

Thin sheets of aluminum alloy 6061-T6 and one type of Advanced high strength steel, transformation induced plasticity (TRIP) steel have been successfully butt joined using friction stir welding (FSW) technique. The maximum ultimate tensile strength can reach 85% of the base aluminum alloy. Intermetallic compound (IMC) layer of FeAl or Fe_3Al with thickness of less than 1 μm was formed at the Al–Fe interface in the advancing side, which can actually contribute to the joint strength. Tensile tests and scanning electron microscopy (SEM) results indicate that the weld nugget can be considered as aluminum matrix composite, which is enhanced by dispersed sheared-off steel fragments encompassed by a thin intermetallic layer or simply intermetallic particles. Effects of process parameters on the joint microstructure evolution were analyzed based on mechanical welding force and temperature that have been measured during the welding process.

1. Introduction

Growing concerns on energy saving and environmental preservations increase the demand for lightweight vehicles. Considerable volumes of advanced high strength steel sheet have been applied into automotive parts in order to reach the objective of both weight reduction and crashworthiness enhancement. However, further weight reduction of 30% or more is hardly achievable with exclusive dependence on the use of thinner steel sheets. Multi-material vehicle structures is an efficient countermeasure against this problem [1], which necessitates the development of reliable and cost-effective dissimilar material joining technique. One of the desired pairs is aluminum alloy and advanced high strength steel, which is highly difficult to be welded together due to their differences in physical and mechanical properties as well as the formation of large amount of brittle intermetallic compounds (IMC) using traditional fusion welding techniques [2–6].

Friction stir welding (FSW), which was first developed by The Welding Institute (TWI) in 1991 [7], has a solid-state nature and therefore exhibits certain advantages over traditional fusion welding methods. First, it can significantly avoid solidification related problems, such as oxidization, shrinkage, porosity, and hydrogen solubility [8]. Second, the associated low heat input can effectively inhibit intermetallic compound (IMC) layer formation, which makes it a promising solution for dissimilar material joining. Several studies have been carried out on FSW of aluminum alloy to steel sheets. Uzun et al. [9] reported the joint strength between 304 stainless steel and Al 6013-T4 with thickness of 4 mm can reach approximately 70% of the base aluminum alloy. Ghosh et al. [10] did FSW of pure Al to 304 stainless steel and the ultimate tensile strength can achieve 82% of Al. Presence of Fe_3Al was reported. Besides, equiaxed and finer grains exist in the stirring zone, which indicate the involved dynamic recrystallization process. Tanaka et al. [11] welded Al7075-T6 to mild steel of the thickness of 3 mm. Tool rotational speed varies from 400 to 1200 rpm under the welding speed of 100 mm/min. The highest tensile strength they can achieve is 333 MPa, which is about 60% of the base aluminum alloy. Moreover, they reported an exponentially increasing relation- ship between the interface strength and the reducing thickness of IMC layer, which has the composition of $FeAl_3$. Lee et al. [12] did experiments on FW of Al6056-T4 to 304 stainless steel with thickness of 4 mm under the rotational speed of 800 rpm and welding speed of 80 mm/min. The thin intermetallic compound layer of 250 nm thickness was analyzed through transmission electron microscopy (TEM) and identified to be $FeAl_4$. Chen and Kovacevic [13] joined Al6061 to AISI 1018 steel sheet with the thickness of 6 mm. Local melting of Aluminum was observed and shear-off steel platelets encompassed by IMC layers of Fe_4Al_{13} and Fe_2Al_5 existed in the weld nugget. Locally partial molten Aluminum was again reported by Jiang and Kovacevic [14] when they did study on the same pair of materials with the same thickness.

* Corresponding author. Tel.: +1 (734) 936 2918; fax: +1 (734) 936 0363.
E-mail address: junni@umich.edu (J. Ni).

http://dx.doi.org/10.1016/j.matdes.2014.02.003
0261-3069/

Intermetallic compounds are found not only in the segregated steel clusters inside the weld nugget but also along the interface between base steel and the nugget. Their constitutions were identified to be Fe_2Al_5 and Fe_4Al_{13}. The severity of IMC reaction depends on locations and more steel is consumed at a distance closer to Aluminum alloy. Movahedi et al. [5] did friction stir lap joint between Al5083 and St-12 mild steel. They found that an intermetallic compound layer with a thickness of less than 2μm will not degrade joint quality. Similar results were suggested by Lee et al. [15] and they reported that 2um IMC layers with the composition of Fe_3Al, Fe_4Al_{13} can contribute to the joint strength. Yilmaz et al. [16] also reported that the Al/Fe interface with a layer of IMC is important to the weld strength but cracks can easily initiate and propagate if the IMC layer is too thick. This statement was further verified by Bozzi et al. [17] when they studied friction stir spot welding of Al6016 to IF-steel and reported that fractures are likely to be generated through the hard IMC tangles when the thickness of IMC layer is larger than 8 μm. In their studies, $FeAl_2$, Fe_2Al_5 and $FeAl_3$ were observed at different positions using TEM. Chen [18] did process parameter study of FSW on Al6061-T651 aluminum alloy to SS400 steel with the thickness of 6 mm. They indicated that rotational and traverse speed are relatively significant FSW process parameters compared to the tool tilt angle or pin diameter. Furthermore, lower rotational speed and transverse speed can result in higher impact values of joint strength. Their maximum tensile strength can reach 76% of the base Al alloy. Kimapong and Watanabe [19] did FSW lap joint on A5083 to SS400 mild steel and reported a maximum shear strength of about 77% of the aluminum base material. FeAl, $FeAl_3$ and Fe_2Al_5 were found in the interface corresponding to different tool tilt angles. Chen et al. [20] suggested the Zn coating on steel could improve the weldability of Al and steel through promoting the formation of Al–Zn low melting point eutectic structure. They also reported in another study [21] on FSW lap joint that the thickness of IMC layer increases from 7.7μm to 58.1 μm with decreasing welding speed, which significantly affect the strength of the joint. The composition was identified to be mainly Fe_2Al_5 and Fe_4Al_{13}. Watanabe et al. [22] joined SS400 mild steel to A5083 Al alloy with the thickness of 2 mm. The maximum tensile strength they have obtained is about 86% of the base Aluminum alloy when 10% of the cross-sectional area of pin was placed in the steel side. The fracture path was along the interface between Al matrix and Fe fragments. IMCs with the composition of FeAl and $FeAl_3$ exist at the upper region of the weld interface.

However, all the aforementioned studies selected either mild steel or austenite stainless steel, both of which have a relatively low yield strength. So far, few open literatures have reported FSW of aluminum alloy to advanced high strength steels (AHSS), which is more desirable in lightweight vehicle structures. AHSS has a much higher mechanical strength and work hardening rate, which is accomplished by their multiple phase microstructure. AHSS consists of four subcategories, i.e. dual phase (DP) steel, transformation induced plasticity (TRIP) steel, complex phase (CP) steel and martensitic steel (MART) [23]. In this work, feasibility of using FSW to join Al 6061 and TRIP 780/800 steel together was investigated and effects of different process parameters were analyzed. Microstructure evolution of the weld was related to mechanical welding forces exerted on the FSW tool and temperature distributions on the workpiece for a thorough understanding of the underlying mechanism.

2. Experiment

Fig. 1(a) shows a schematically axonometric view of the whole FSW experimental arrangements and Fig. 1(b) shows a more detailed cross-sectional view perpendicular to the weld line. TRIP 780/800 steel sheets with the thickness of 1.4 mm were provided by the United States Steel Corporation. Its yield strength (YS) is 780 MPa, which is more than three times of that of Al6061. According to Watanabe et al. [22], steel should be put in the advancing side for admissible joining configurations. The thickness of aluminum alloy Al6061-T6511 is 1.5 mm and its chemical compositions and mechanical properties are listed in Table 1, where UTS stands for ultimate tensile strength.

Blue[1] lines in Fig. 1 indicate the contour of the FSW tool, which consists of a conically tapered non-threaded pin. Specific dimensions of the tool are shown in Fig. 2. To avoid overheating of aluminum, the FSW tool should be shifted towards aluminum. However, partial of the pin need to remain in the steel side to actually stir both materials together. The parameter of tool offset is therefore introduced here as the distance between the tool axis and the faying surface of the two materials. Larger tool offset means the tool is more into aluminum. Since part of the FSW tool will be immersed in the steel side and subjected to severe frictional conditions, refractory materials such as tungsten carbide [24–27], tungsten–rhenium [28], Si_3N_4 [29] and polycrystalline cubic boron nitride (PCBN) [30–32] are required for the tool. In our study, tungsten carbide with 10% cobalt content was selected for its good wear resistance and much lower cost compared with PCBN.

Below the workpieces is a replaceable backing plate made of mild steel, where four holes with diameter of 1 mm were drilled for mounting thermocouples. Type K thermocouples, shown as red spots in Fig. 1, are located symmetrically to the weld line and measure the temperature of the workpiece back surface at distances of 1 mm and 5 mm away from the abutting edge.

The workpiece and replaceable backing plate were assembled onto a specially designed fixture, which was further mounted onto a dynamometer (Kistler 9255B). The dynamometer was used to measure the mechanical welding force in both vertical direction F_z and the direction along joint line F_x. All FSW experiments were performed on the high stiffness M.S. Machining Center under displacement control. Two levels of rotational speed, 1200 rpm and 1800 rpm were investigated under three levels of welding speed and two levels of tool offset. As shown in Table 2, a total of 12 welding conditions were carried out in this study and each condition was repeated three times for average and error bar calculation. R, FT and Offset are abbreviations for rotational speed, welding speed and tool offset respectively, which are frequently referred to in the figures shown in following sessions.

Microstructural analysis using both optical microscopy (OM) and Scanning Electron Microscopy (SEM) were performed on the joint cross sections perpendicular to the weld line. Composition of the interface layer was analyzed using X-ray diffraction (XRD) technique. Tensile specimens perpendicular to the weld line were prepared according to the ASTM: E8 standard. Their specific shape and dimensions are shown in Fig. 3. Thickness of the tensile specimens is the same as the original workpiece but with a transition thickness in the weld area, which was located almost right in the center. All the tensile tests were conducted on the MTS Insight 10 tensile machine at a strain rate of 10^{-3}.

3. Results and discussion

3.1. Microstructure overview and material flow visualization

A typical optical macroimage of the joint cross section perpendicular to the weldline is shown in Fig. 4, which reveals a good

[1] For interpretation of color in Fig. 1, the reader is referred to the web version of this article.

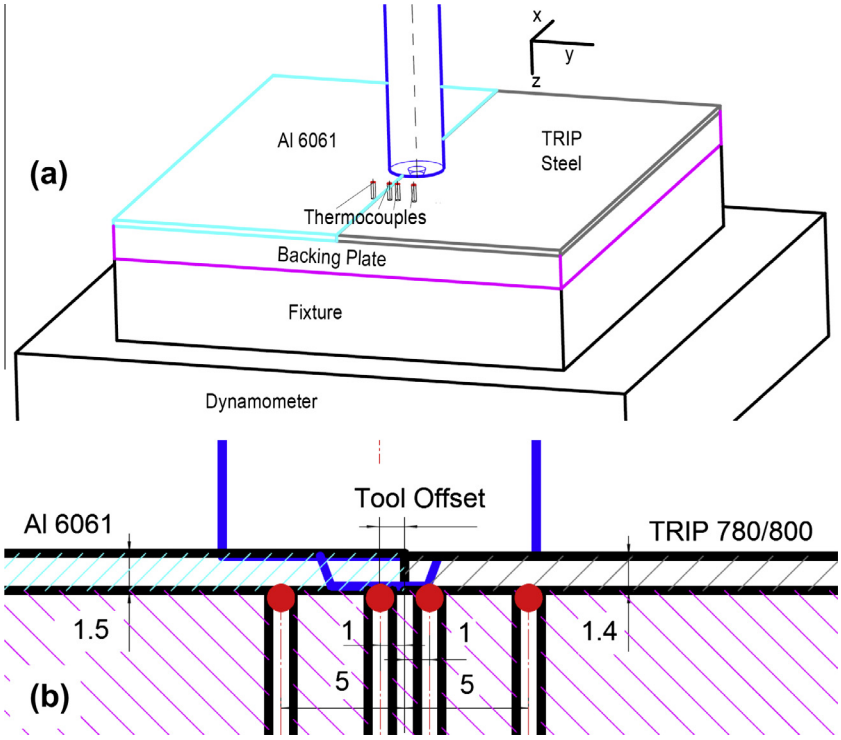

Fig. 1. Schematic illustration of the FSW experimental configuration (a) axonometric view of the whole FSW experimental configuration; (b) cross-sectional view perpendicular to the weld line (unit: mm).

Table 1
Chemical composition and mechanical properties of the Al6061-T6511 alloy.

Chemical composition							Mechanical properties	
% Si	% Mg	% Fe	% Cr	% Cu	% Zn	% Ti	YS (MPa)	UTS (MPa)
0.6	1	0.35	0.42	0.27	0.12	0.08	245	283

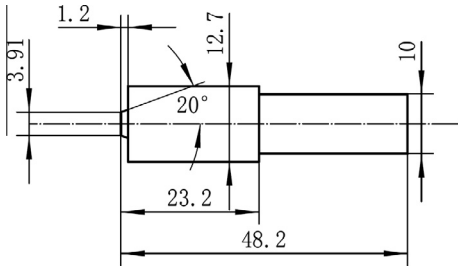

Fig. 2. Detailed dimensions of the FSW tool (unit: mm).

Table 2
Process parameters studied in FSW of Al 6061 to TRIP steel.

FSW condition	Rotational speed (R) (rpm)	Welding speed (FT) (mm/min)	Tool offset (Offset) (mm)
1	1200	30	1.03
2	1200	60	1.03
3	1200	90	1.03
4	1200	30	1.63
5	1200	60	1.63
6	1200	90	1.63
7	1800	60	1.03
8	1800	90	1.03
9	1800	120	1.03
10	1800	60	1.63
11	1800	90	1.63
12	1800	120	1.63

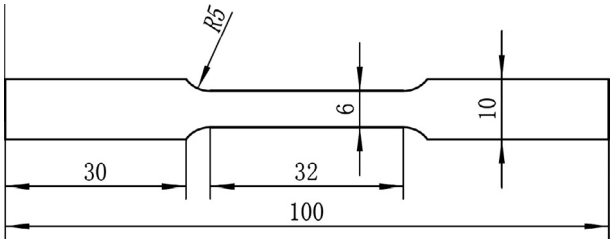

Fig. 3. Shape and dimensions of the tensile specimens from the weld (unit: mm).

weld quality containing neither visible pores nor cracks. A number of black spots in addition to sheared-off steel fragments can be observed to scatter all over the weld nugget with various sizes and morphologies. A continuous steel strip was peeled off from the base TRIP steel side and extruded into aluminum matrix, which illustrates the pattern of material flow during this FSW process. In the advancing side, the materials from aluminum region has been stirred over and pushed against steel. Vertical force exerted by the pin of FSW tool tends to press this part of aluminum and steel downward, which was restricted by the backing plate when they reached the bottom of the nugget. Since total length of the pin is less than the thickness of the workpiece, the materials at the bottom of advancing side were therefore squeezed and move horizontally into aluminum side through the "strait" formed by the end surface of the pin and the backing plate. The softer properties of aluminum matrix make it easier for the TRIP steel to penetrate. TRIP steel will tend to follow the flow of aluminum in the retreating side once being transported through the "strait" as the tool moves forward. An upward motion was clearly exhibited by the embedded TRIP steel in the retreating side. According to Guerra et al. [33] and Colligan [34], the materials tend to be carried away and deposited in the wake of the pin as the tool continuously moves forward. Since a lot more frictional heat are generated by

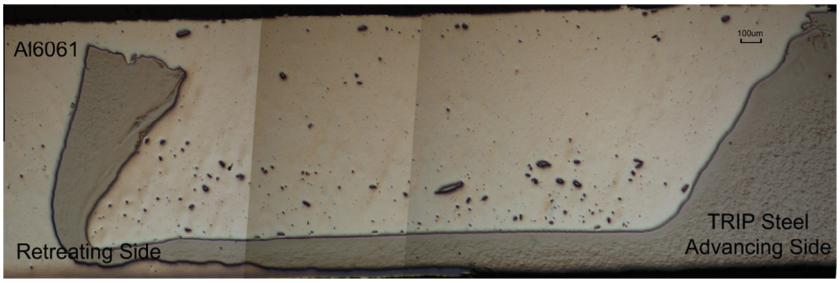

Fig. 4. Typical optical macroimage of the weld cross section (process condition rotational speed of 1800 rpm; welding speed of 60 mm/min; tool offset of 1.63 mm).

the shoulder of the rotating tool, top region of the weld will be under a higher temperature and therefore has smaller flow stress than the bottom does. Consequently, relatively larger amount of materials at the top area are moved backward and the materials in the bottom will then try to occupy this available space due to the pressure exerted by the tool. In other words, materials will tend to flow upward. Similar results regarding the upward motion have also been reported by Reynolds [35] and Coelho et al. [36].

3.2. Analysis of Al–Fe interface in the advancing side

In order to examine the metallurgical bonding conditions in the advancing side, scanning electron microscopy (SEM) was employed for higher magnified views. Fig. 5 shows SEM images of the Al–Fe interface under different welding speeds while maintaining the rotational speed of 1200 rpm and tool offset of 1.03 mm. A distinct interfacial layer with a different color from either steel or aluminum can be observed, which indicates a newly formed phase of intermetallic compounds (IMC). The intermetallic layer has a relatively smooth boundary in the dark aluminum side compared with the wavy morphology of the boundary in the bright steel side. These irregularities in steel side could be explained considering crystallization and growth of the IMC. Valleys in the steel side boundary correspond to the initially formed nuclei of IMC, which tend to absorb Al and Fe atoms that have diffused over and grow in both lateral and depth directions under appropriate temperature and pressure conditions. Regions of steel where the lateral growth of IMC nuclei did not reach will therefore left as wave peaks in the boundary. In some extreme cases, these peaks appear in needle shapes, as shown in the bottom region of Fig. 5(a). Smooth boundary in the aluminum side also indicates that aluminum diffusion is unlikely to be the rate determining step during this IMC formation process. Despite coarse boundaries, overall thickness of this interface layer becomes smaller as the welding speed increases, which can be observed in Fig. 5.

The relationship between interlayer thickness and welding speed is consistent regardless of variations on either rotational speed or tool offset, as shown in Fig. 6 where a higher rotational speed of 1800 rpm and larger tool offset of 1.63 mm were applied. The growth kinetics of this interlayer was further quantitatively studied by measuring its thickness under different sets of process parameters. Considering the unsmooth morphology near steel side, measurements were taken at three different subareas of each interface and in each subarea three peaks and valleys of the wavy boundary were selected. Average values of thickness t were calculated in each subarea and plotted with respect to welding speeds v in logarithm scale as shown in Fig. 7. It can be seen that higher rotational speed is able to increase the interlayer thickness. Moreover, larger portion of the tool immersed in aluminum yields a thinner layer. All these phenomena can be explained from the force and temperature measurements during the process, which will be shown in the following sessions.

A linear dependence of $\ln(t)$ on $\ln(v)$ can be observed in Fig. 7. By further calculating the fitting slope, relationships between layer thickness t and welding velocity v under different rotational speeds and tool offsets were summarized in Table 3. Since duration of welding stage with the same welding length is inversely proportional to v, the inverse relationship or inverse parabolic relationship between the thickness and the welding speed can be approximately interpreted as linear or parabolic relationship with time. According to Bouche et al. [37], growth of the intermediate phases will follow linear kinetics if it is governed by chemical reactions or it will follow parabolic kinetics if the rate determining step is interdiffusion. The linear relationship under rotational speed of 1200 rpm and tool offset of 1.03 mm indicates a reaction controlled interphase growth while the process under other three conditions are likely to be controlled by diffusion. Furthermore, the wavy boundary in the steel side indicates iron atom diffusion in TRIP steel rather than aluminum atom diffusion is the rate determining step. These different kinetics suggest the formation of different types of IMC.

Composition of the IMC layer was identified using X-ray Diffraction (XRD) technique and results are shown in Fig. 8. The most likely existed phases are determined based on the figure of merit

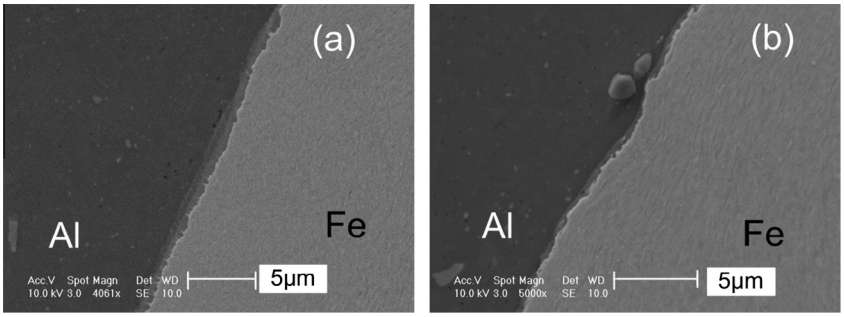

Fig. 5. SEM images of the Al–Fe interface in the advancing side of weld samples under rotational speed of 1200 rpm, tool offset of 1.03 mm and different welding speeds: (a) 30 mm/min; (b) 60 mm/min.

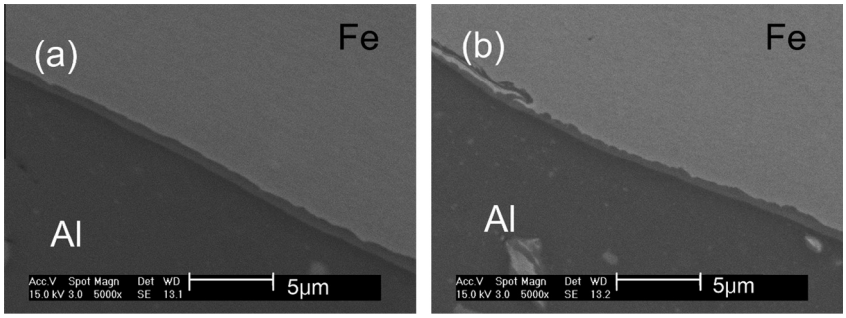

Fig. 6. SEM images of the Al–Fe interface in the advancing side of weld samples under rotational speed of 1800 rpm, tool offset of 1.63 mm and different welding speeds: (a) 60 mm/min; (b) 90 mm/min.

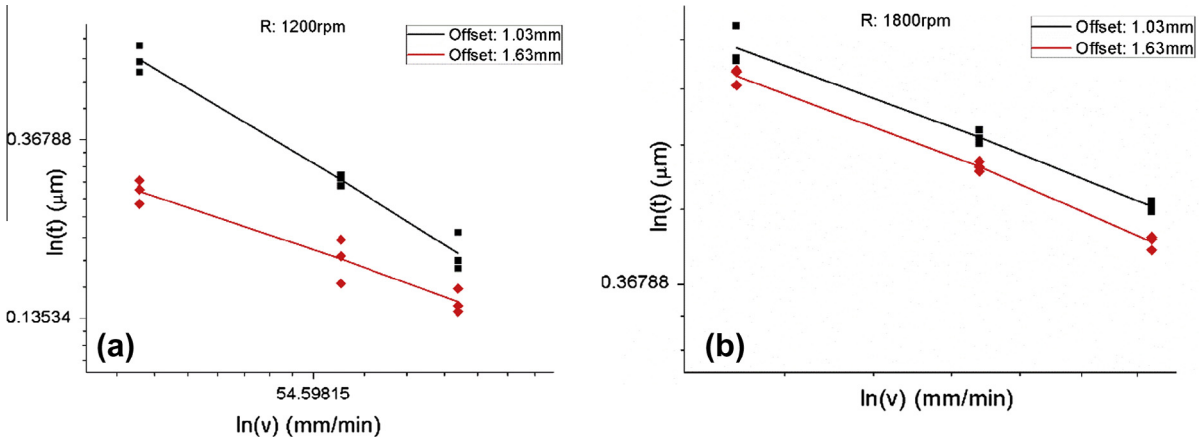

Fig. 7. Relationships between thickness of the interlayer t and welding speed v under different tool offsets and rotational speeds (a) 1200 rpm; (b) 1800 rpm.

Table 3
Dependence of the interlayer thickness t (μm) on the welding speed v (mm/min).

(rpm)	Tool offset: 1.03 mm	Tool offset: 1.63 mm
Rotational speed: 1200	$t \propto \frac{1}{v}$	$t \propto \frac{1}{\sqrt{v}}$
Rotational speed: 1800	$t \propto \frac{1}{\sqrt{v}}$	$t \propto \frac{1}{\sqrt{v}}$

(FOM) values calculated by the XRD analysis software JADE. It can be seen that welding speeds has no influence on the type of IMC that is going to form. Furthermore, only under the condition where rotational speed is 1200 rpm and tool offset is 1.03 mm can the FeAl phase be generated. Fe_3Al is formed under all other conditions, which are in agreement with the above results on interlayer growth kinetics.

3.3. Nugget characteristics

A series of SEM images taken at different positions in the weld nugget are shown in Fig. 9. Steel fragments of various sizes and morphologies can be observed not only inside but also outside of the stirred over steel strip. More importantly, all of them are encompassed by an intermetallic layer, which implies chemical reactions occurred instead of simply mixing between these sheared off steel platelet and aluminum matrix. Furthermore, it is not only the steel fragments that exist, particles of intermetallic compounds also distribute independently in the nugget with much smaller size, which is usually around 2–5 μm for the largest dimension. Some of them may fall off during polish process and leave black holes in these figures. Formations of these particles were most likely through reaction between sheared off small steel particles and aluminum matrix. In these cases, the steel particles are completely consumed. Since intermetallic compound (IMC) possesses a much higher hardness than either Al or Fe, the nugget could be considered as an IMC enhanced aluminum matrix. This conclusion was later verified through tensile tests, where the nugget exhibited satisfying strength compared with other regions of the weld.

3.4. Temperature distribution and thermal history

Temperature distribution on the back surface of workpiece under different process parameters was shown in Figs. 10 and 12–14. X-axis represents relative locations of the thermocouples with regard to the abutting edge. Aluminum side is denoted as negative values so that the ordinal positions of temperature points in these figures are visually consistent with those in the experimental setup shown in Fig. 1. Y-axis represents the peak temperature that has been recorded at this position during the whole FSW process. Temperature measuring points are symmetric to the abutting edge. However, since FSW tool was shifted more into Al side in all our experiments, they are asymmetric to the tool, which is also the heat source. It can be seen that the temperature at 1 mm position in Al side is slightly higher than that in steel side, which can be interpreted by the closer distance to the FSW tool. Besides, according to Nandan et al. [38], local heat generation rate during FSW can be approximately given by:

$$dq \approx wr(\delta\mu_f p + (1-\delta)\tau_y)dA \quad (1)$$

where w is the tool rotational speed, r is the radial distance from the tool axis, δ represents the extent of slip, μ_f is the friction coefficient, p is the local pressure corresponding to the mechanical welding

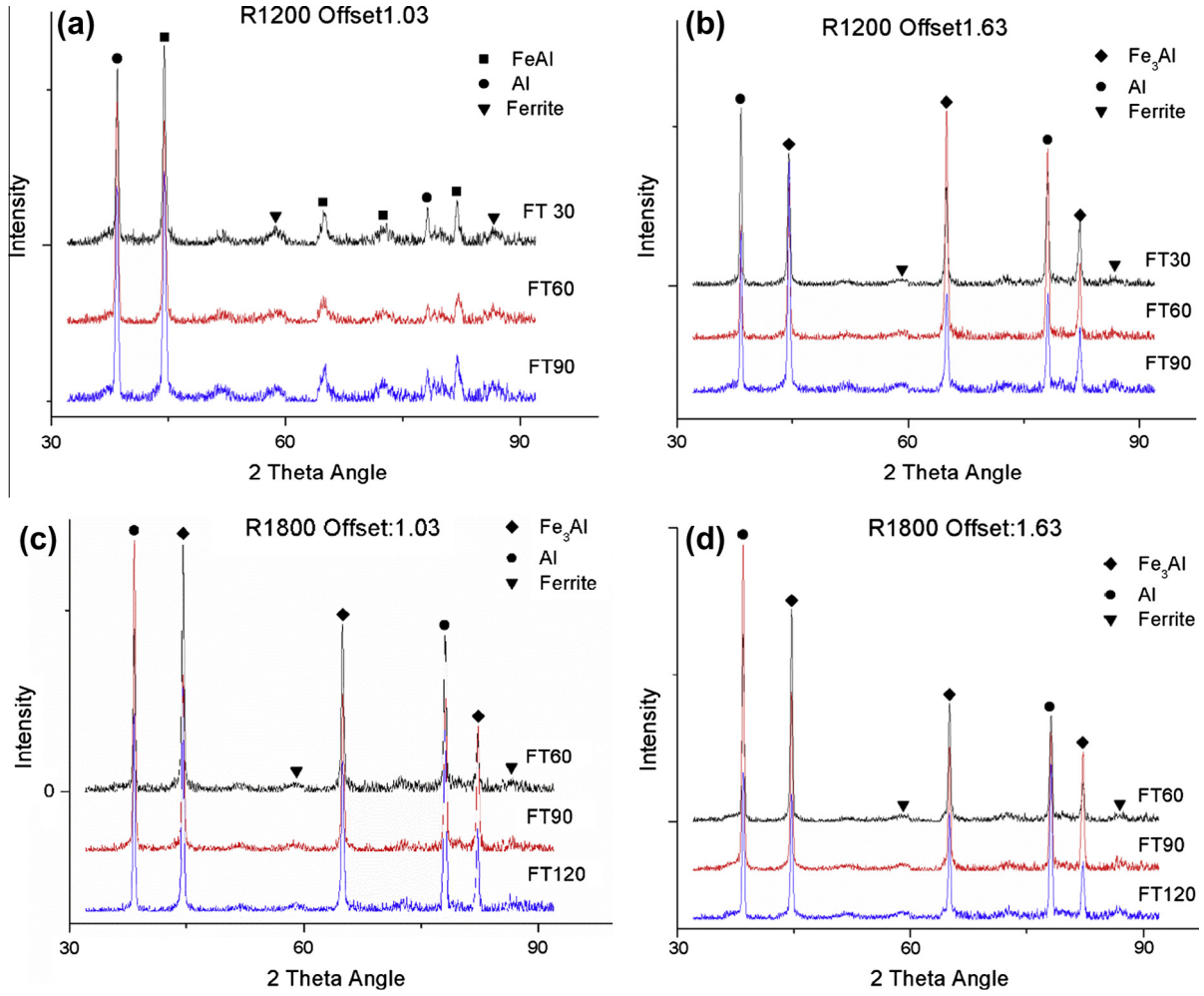

Fig. 8. XRD diffraction patterns of the interfacial layer under different process parameters where FT represents different welding speeds (a) rotational speed: 1200 rpm; tool offset: 1.03 mm; (b) rotational speed: 1200 rpm; Tool offset: 1.63 mm; (c) rotational speed: 1800 rpm; tool offset: 1.03 mm; (d) rotational speed: 1800 rpm; tool offset: 1.63 mm.

force and τ_y is the shear yield strength of the stirred material. When considering FSW of dissimilar materials in this study, the heat generation comes from friction and plastic deformation of both materials. Therefore, Eq. (1) can be revised as follows:

$$q \approx w\left\{\iint_{\mathrm{Al}} r\left(\delta_{\mathrm{Al}}\mu_{f\mathrm{Al}}p + (1-\delta_{\mathrm{Al}})\tau_{y\mathrm{Al}}\right)dA_{\mathrm{Al}} + \iint_{\mathrm{Fe}} r\left(\delta_{\mathrm{Fe}}\mu_{f\mathrm{Fe}}p + (1-\delta_{\mathrm{Fe}})\tau_{y\mathrm{Fe}}\right)dA_{\mathrm{Fe}}\right\} \quad (2)$$

Since the original thickness of Al sheet is 0.1 mm larger than that of steel, which requires the shoulder of the tool to penetrate Al for 0.1 mm before it can rub against the upper surface of steel. Accordingly, a lot more heat is generated on tool shoulder in Al side through plastic deformation in addition to friction. On the other hand, heat generated by steel plastic deformation comes primarily from the small portion of the pin immersed in steel, which is relatively small and accounts for the lower temperature at 1 mm point in steel side. The temperature at 5 mm position in Al side is greatly higher than that in steel side due to the much higher thermal conductivity of aluminum compared with steel.

Fig. 10 compares the temperature distribution under different welding speeds with rotational speed of 1800 rpm and tool offset of 1.63 mm. It can be seen that welding speed has an insignificant effect on the temperature distribution in Al side. Similar results were also reported by Barnes et al. [28]. Smaller welding speed can slightly increase the temperature in steel side, which could be explained from the aspect of thermal history. Fig. 11 shows the effect of welding speed on thermal history at 1 mm position in Al side under the same rotational speed and tool offset as before. It can be seen that although welding speed could hardly influence the peak temperature, larger welding speed can directly reduce the high temperature period and elevate heating and cooling rate. Consequently under a small welding speed, heat generated in Al side can have a longer time to be conducted into steel and raise the temperature. Similar results regarding the effect of welding speed on temperature distribution are shown in Fig. 12, where a smaller rotational speed of 1200 rpm was applied. Furthermore, the thermal history result helps explain the effects of welding speed on the IMC layer thickness in advancing side. Since formation of IMC layer relies on diffusion and reaction of aluminum and iron atoms, longer high temperature period enables generation of larger amount of IMC. Accordingly, lower welding speed can increase the thickness of the IMC layer as shown in Fig. 7.

Effects of different rotational speeds on the temperature distribution are shown in Fig. 13. It can be observed that temperature in both aluminum and steel side is higher under a larger rotational speed and this conclusion is consistent regardless of welding

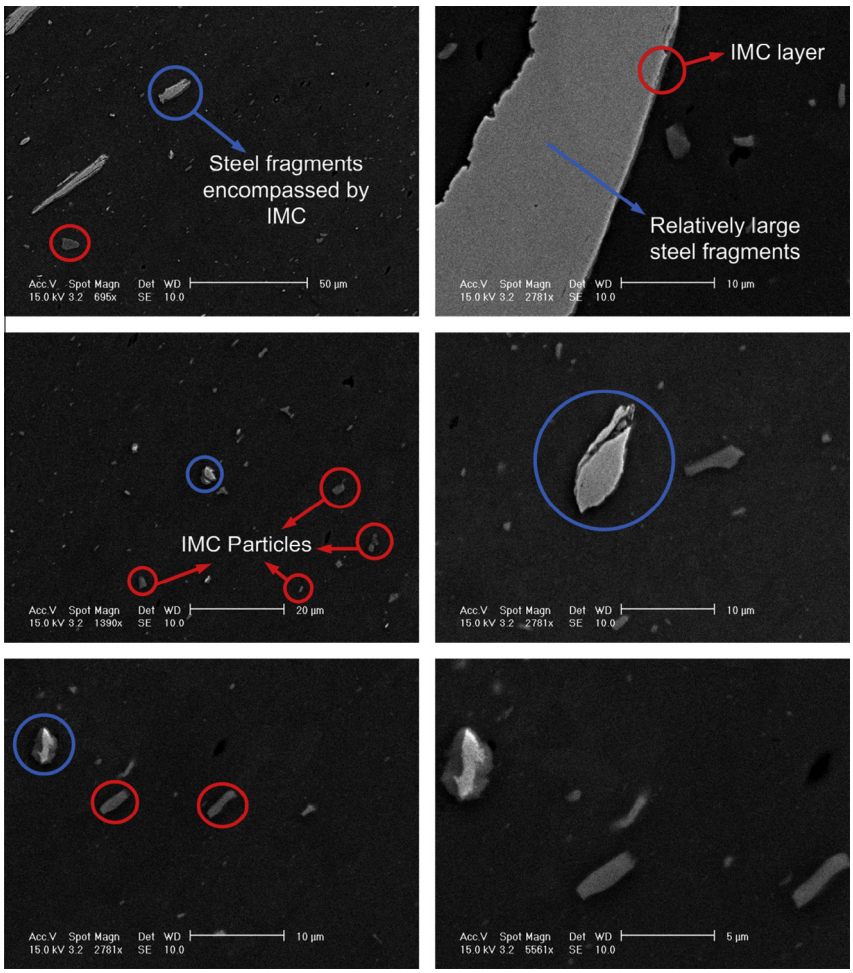

Fig. 9. SEM images taken at different positions in the weld nugget: red circles are some representative IMC particles while blues ones correspond to steel fragments encompassed by IMC layer. (For interpretation of the references to colour in this figure legend, the reader is referred to the web version of this article.)

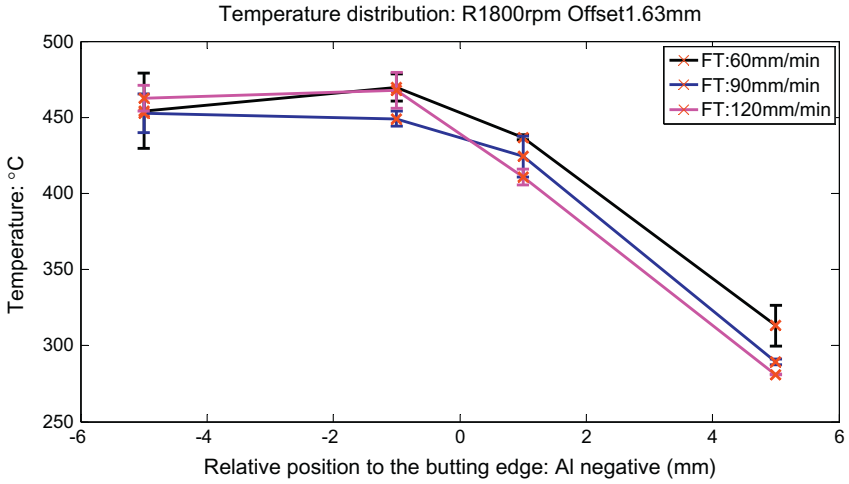

Fig. 10. Temperature distribution under different welding speeds with the rotational speed of 1800 rpm and the tool offset of 1.63 mm.

speeds. Influence of rotational speed on temperature will accordingly affect IMC layer growth. Since higher temperature help facilitate diffusion and reaction, higher rotational speed can increase the interlayer thickness as shown in Fig. 7.

Fig. 14 shows effects of different tool offsets on temperature distribution. It can be seen that the overall temperature will increase when the tool is shifted more towards aluminum, which further indicates that the average heat generation density in the aluminum side is larger than that in steel side under our current configuration. However, the general trend of temperature variation is barely consistent at the 1 mm point in steel side, which can be explained based on the relative position of FSW tool and

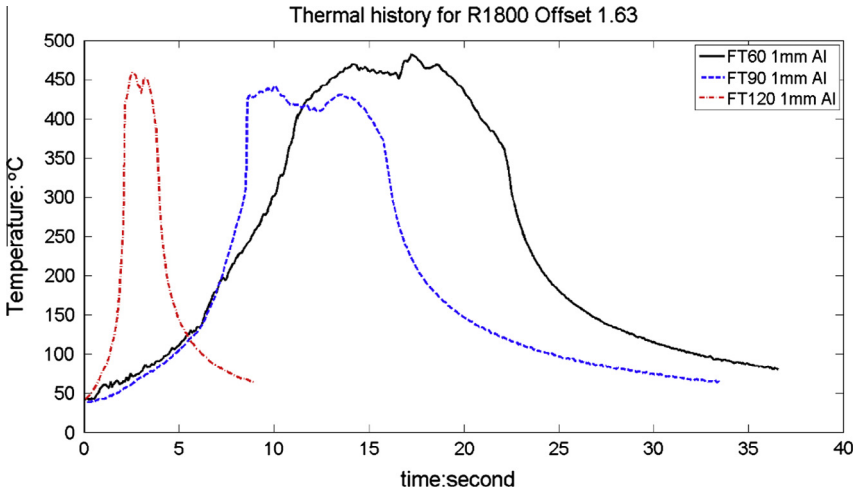

Fig. 11. Thermal history at 1 mm position in Al side under different welding speeds with the rotational speed of 1800 rpm and tool offset of 1.63 mm.

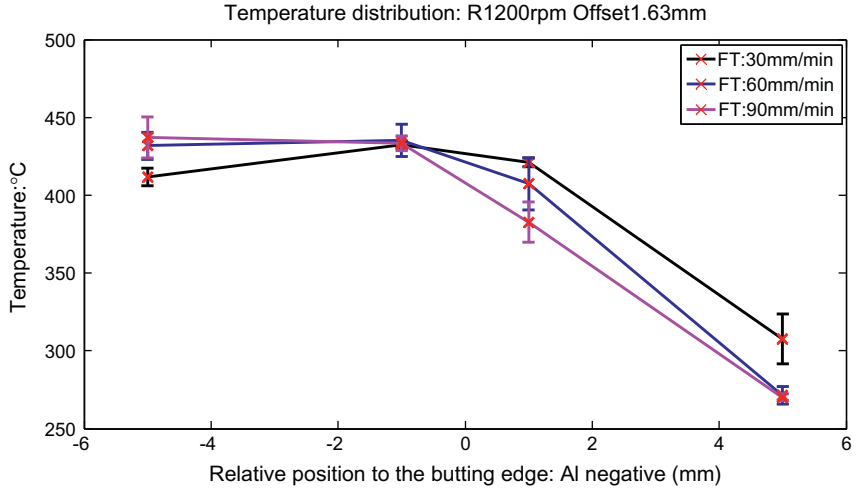

Fig. 12. Temperature distribution under different welding speeds with the rotational speed of 1200 rpm and the tool offset of 1.63 mm.

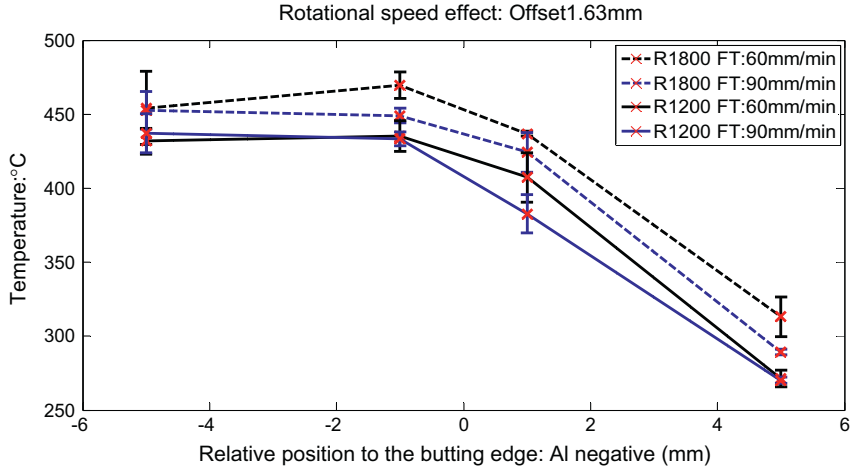

Fig. 13. Temperature distribution under different rotational speeds with the tool offset of 1.63 mm.

this temperature measuring point. As can be seen from Fig. 1, under a tool offset of 1.03 mm the stirring edge of the pin is right above this temperature measuring point. This position receives not only the frictional heat from tool shoulder but also dissipated plastic energy generated by the pin, which has the largest value at the pin periphery. On the other hand, when the tool is moving

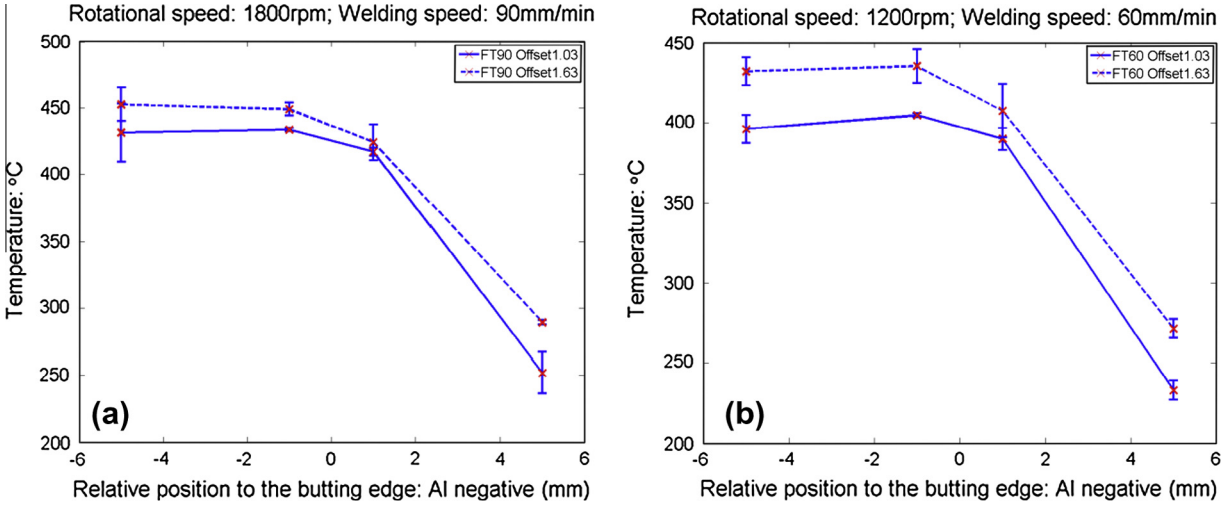

Fig. 14. Effects of different tool offsets on the temperature distribution (a) rotational speed of 1800 rpm with welding speed of 90 mm/min; (b) rotational speed of 1200 rpm with welding speed of 60 mm/min.

further into aluminum by 0.6 mm, the stirring edge of the pin will be away from the 1 mm point in steel side and makes less contribution of heat conduction, which results in a relatively lower temperature.

3.5. Mechanical welding force

FSW experiments conducted in this study are displacement controlled, the force exerted by FSW tool on workpiece will therefore vary depending on different process conditions. Fig. 15 compares the vertical force F_z reached during stable welding stage, which represents the required pressure for confining the material within the weld when translating the tool. *X*-axis represents welding speed. Rotational speeds are distinguished by colors and tool offsets are expressed using different line types. Overall, F_z increases slightly with the traverse welding speed whereas the relationship is weak in the studied in this work, which is in agreement with the temperature measurement results. Larger rotational speed and tool offset can effectively reduce F_z.

Fig. 16 shows the lateral moving force F_x reached during stable welding stage under different sets of process parameters. Similar to the trend of vertical force, the lateral force F_x increases slightly with the welding speed but is not sensitive to this factor. On the other hand, higher rotational speed and especially tool offset can effectively reduce the lateral moving force F_x.

3.6. Relationship between process parameters and the Al–Fe interface

Formation and growth of intermetallic compound at the interface of dissimilar materials basically contain three stages [39]. The first stage involves generation of supersaturated solid solution due to diffusion of atoms in the interface. This solid solution will transform into IMC in the second stage when its composition reaches to the saturation level at corresponding temperature and pressure conditions. In the third stage, solute atoms will diffuse into the formed IMC layer for it to grow gradually. Several researches have been conducted regarding the interlayer formation and growth between molten Al and solid Fe [37,40–43]. According to their studies, Fe_2Al_5 and $FeAl_3$ are more likely to be formed in the temperature range of 700–900 °C. On the other hand, for IMC with low aluminum composition, basically FeAl and Fe_3Al, can only be formed at a higher temperature of over 1000 °C. The Al–Fe phase diagram [44] under atmospheric pressure is shown in Fig. 17, which indicates the formation of Fe_3Al at the temperature of about 552 °C by a first order reaction of FeAl while FeAl is formed through a peritectic reaction under a much higher

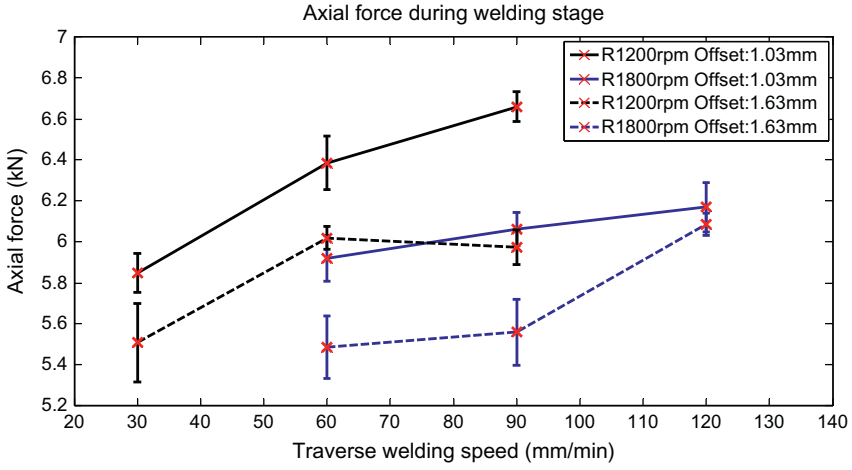

Fig. 15. Effects of various process parameters on the axial force F_z during stable welding stage.

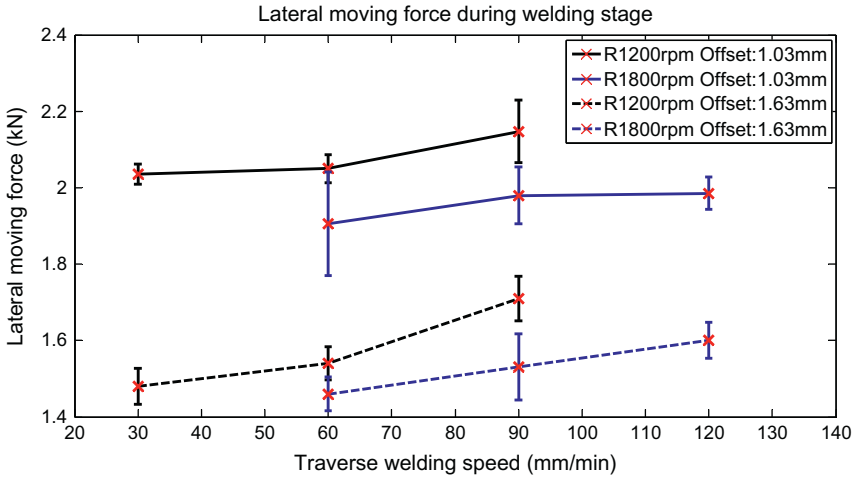

Fig. 16. Effects of various process parameters on lateral moving force F_x during stable welding stage.

temperature of around 1310 °C. However, based on the temperature measurement results shown in Figs. 10–14, the highest temperature at the back surface of the workpiece in all the experiments conducted in this study was less than 500 °C. Since the thickness of Al sheet is 1.5 mm and TRIP steel is 1.4 mm, the temperature variation can hardly achieve 500 °C in this thin region. In order to account for the formation of FeAl and Fe_3Al at this relatively low temperature, effects of pressure which corresponds to the mechanical welding force during FSW needs to be taken into consideration. It was reported in [39] that an increase in pressure can cause formation of interface layer at lower temperature under constant diffusion time. During FSW process, both vertical and lateral welding force will raise the pressure in the weld and therefore promote intermetallic reaction. Furthermore, during FSW, materials near the pin are suffering from severe plastic deformation at a high strain rate, which also enhances diffusion and IMC reaction. It is suggested that short-circuiting along static and moving dislocations, grain boundaries and cracks generated during deformation are the main causes for this diffusion enhancement [45]. These defects consequently facilitate atoms from different species to occupy available lattice sites of the original species and form IMC. In summary, the formation and growth of IMC layers depend closely on temperature, mechanical welding force and material deformation status, all of which are determined by process parameters. Higher rotational speed can effectively increase the temperature in the weld, reduce welding force in both vertical and lateral direction according to the previous temperature and welding force measurement results. In addition, it can also increase the material strain rate, which should be positively correlated with the line speeds of the corresponding points on the tool. Therefore higher rotational speed can enhance the diffusion process to a great extent and more IMC was generated. Welding speed has an inappreciable effect on either temperature distribution or mechanical welding force. Furthermore, its influence on the material deformation rate is

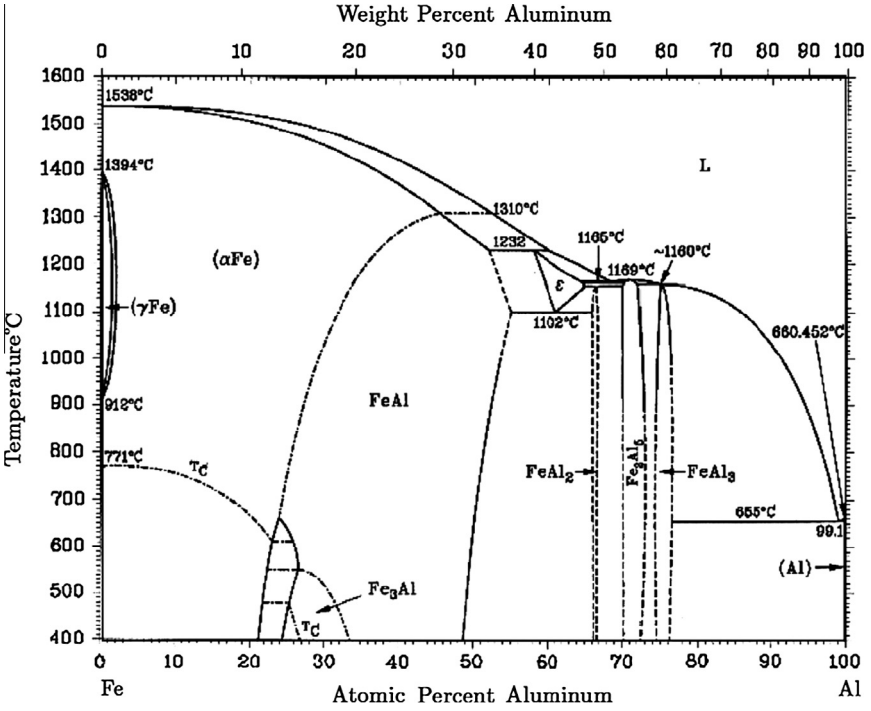

Fig. 17. Al–Fe phase diagram under atmospheric pressure [44].

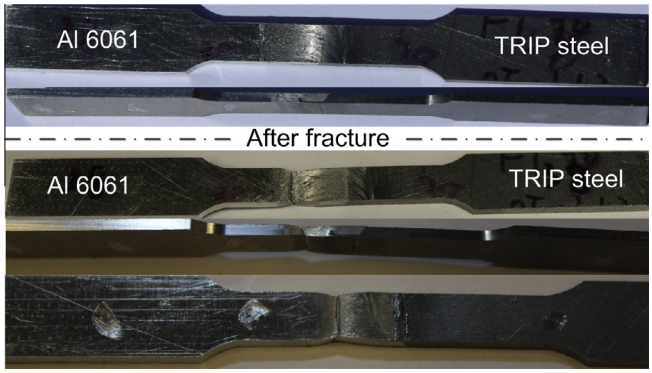

Fig. 18. Tensile specimen before and after breakage (process conditions: rotational speed of 1800 rpm; welding speed of 90 mm/min; tool offset of 1.63 mm).

negligible compared with that of tool rotating speed. As a result, welding speed could hardly affect diffusion and IMC reaction process and consequently the composition of the IMC layer. However, extended high temperature period under lower welding speed was shown in the thermal history results, which allows for longer diffusion time and therefore generation of thicker IMC layers. Smaller tool offset means larger fraction of steel is involved in the stirring process and react with aluminum, which will overall increase the interlayer thickness. It was shown that under the lower rotational speed of 1200 rpm and smaller tool offset of 1.03 mm, FeAl was formed at the interface, which was different from the Fe_3Al obtained under all other conditions. This could be explained from following aspects. Smaller tool offset has been shown to increase welding force in both vertical and lateral direction and can therefore elevate the pressure in weld nugget, which contributes to IMC reaction. However, the relatively low temperature results from both small tool offset and low rotational speed retards further diffusion of iron atoms into the initially formed IMC layer with the composition of FeAl. As a result, FeAl can hardly be transformed into Fe_3Al under insufficient concentration of iron atoms and leaves as interlayer composition after the weld. Temperature distribution is higher under all other conditions and therefore allows for the formation of Fe_3Al.

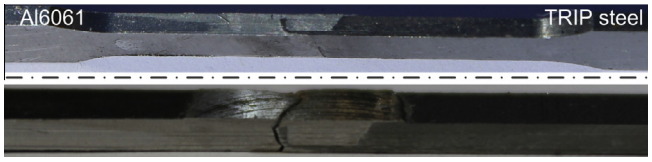

Fig. 19. Tensile specimen fractured along the interface between the outside boundary of the stirred over steel strip and aluminum matrix (process conditions: rotational speed of 1800 rpm; welding speed of 120 mm/min; tool offset of 1.03 mm).

3.7. Joint strength

The highest ultimate tensile strength (UTS) of FSW joints obtained in this study was 240 MPa, which is about 85% of the base Al alloy. One of the tensile specimens obtained under rotational speed of 1800 rpm, welding speed of 90 mm/min and tool offset of 1.63 mm is shown in Fig. 18, where the upper two photos were taken before tensile test and the lower three were after fracture. Necking and fracture can be clearly seen to occur in the heat affected zone of Al, which is apart from the weld nugget and abutting edge. The loss of strength in this region is likely to be caused by dissolution and over-aging of fine precipitates that form inside Al6061 after T6 aging.

On the other hand, specimens under most other conditions exhibited a different failure mode and a typical one is shown in Fig. 19. Necking is hardly distinguishable in this case. Special attention should be paid to the fracture path, which was along the interface between the outside boundary of the stirred over steel strip and aluminum matrix. It was also be noticed that none of the specimens fractured inside the nugget, which can be considered as metal matrix composite where aluminum is the matrix and the IMC corresponds to the reinforcement. In order to develop further understanding of the observed fracture path, SEM images were taken at different positions along all the observable Al–Fe interfaces and the results are shown in Fig. 20.

Position 1 shows the Al–Fe interface in the advancing side, which has been analyzed in previous sessions. Notice that under all of the investigated process conditions, the maximum thickness of the IMC layer in this area was less than 1 μm and none of the specimen

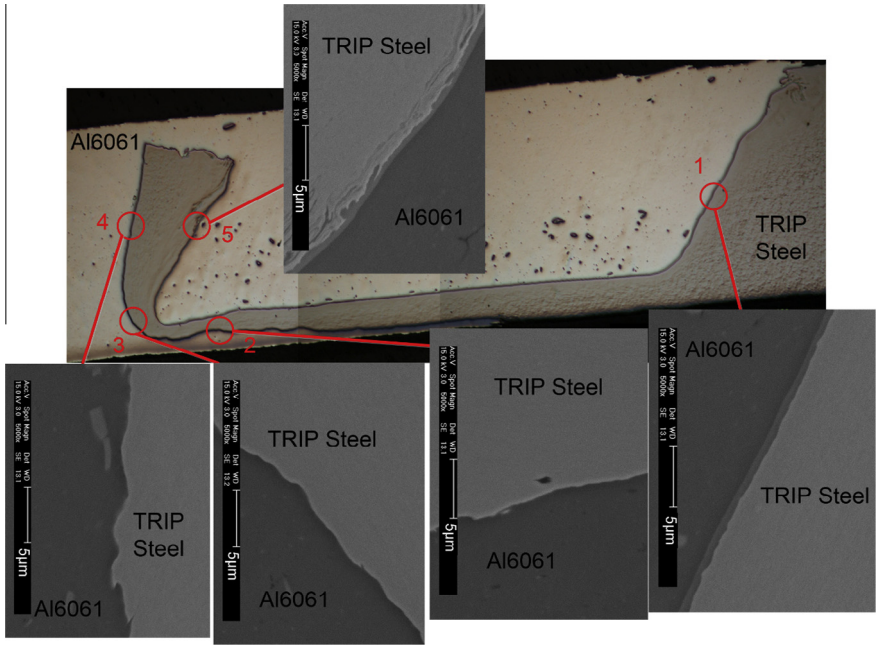

Fig. 20. SEM images at different positions along all the observable Al–Fe interfaces (process conditions: rotational speed of 1800 rpm; welding speed of 60 mm/min; tool offset of 1.63 mm).

broke at this location. On the other hand, it can be observed that no IMC layer formed at positions 2, 3, 4 on the outside boundary of the stirred over steel strip, which are the actual locations where most of the fractures occurred. In this region, steel and aluminum are indicated to be merely adhered to each other. Another SEM image taken at position 5 inside of the stirred over steel strip shows again the presence of IMC layer and there was no failure at this position as well. Formation of a thin layer of IMC is therefore shown to be beneficial for joint strength. Besides, in this study the composition of the IMC layer was identified to be either FeAl or Fe_3Al, which are iron rich IMCs and less brittle than aluminum rich ones, including $FeAl_2$, Fe_2Al_5 and $FeAl_3$ [42]. Besides, iron rich IMCs possess a good corrosion resistance [46,47], which is highly desirable for Al–Fe joints. It can be anticipated that with such a continuous thin intermetallic layer connecting aluminum and steel together, the related corrosion problem can be promisingly attenuated.

4. Conclusions

Friction Stir Welding (FSW) technique was successfully applied to joining of Al6061 alloy to TRIP 780/800 steel and the maximum tensile strength obtained is about 85% of the base Al alloy. Microstructure analysis was related to different sets of process parameters based on measurements of mechanical welding force and temperature distribution. Main findings of this study are summarized as follows:

- In the advancing side, stirred over aluminum was pushed against base steel and a thin IMC layer of less than 1 μm was formed at the interface due to diffusion and reaction.
- Welding speed had an insignificant effect on mechanical welding force, temperature distribution and material strain rate and therefore the IMC layer composition. However, higher welding speed can shorten high temperature period and thus reduce the interlayer thickness.
- Higher rotational speed and larger tool offset can elevate the overall temperature distribution in the weld and reduce the required vertical and lateral force for translating the tool along joint line. Accordingly, they can also influence the composition of the formed IMC layer. Under a low rotational speed and small tool offset, FeAl was formed instead of Fe_3Al, which was formed under all other conditions.
- Sheared-off steel fragments encompassed by a thin layer of IMC or simply IMC particles are unevenly distributed in the weld nugget, which can be considered as metal matrix composite with aluminum as the matrix and IMC as the reinforcement.
- A thin IMC layer with the thickness of less than 1 μm and the composition of FeAl or Fe_3Al can contribute to joint strength. The Al–Fe adhering interface on the outside boundary of the stirred over steel strip was shown to be the most vulnerable location of the weld.

Future works will further consider the integrity of the weldment through detailed fractographic studies and the cross section will be etched to reveal the grain structures for both steel and aluminum with different etching reagents. A finite element model will be developed for predicting the welding force and temperature distribution, which will serve for optimization of the process parameters.

Acknowledgement

This work is supported by the CERC-CVC U.S.–China Program of Clean Vehicle under Award Number DE-PI0000012.

References

[1] Sakiyama T, Murayama G, Naito Y, Saita K, Oikawa YMH, Nose T. Dissimilar metal joining technologies for steel sheet and aluminum alloy sheet in auto body. Nippon steel technical report, 2013.
[2] Ogura T, Saito Y, Nishida T, Nishida H, Yoshida T, Omichi N, et al. Partitioning evaluation of mechanical properties and the interfacial microstructure in a friction stir welded aluminum alloy/stainless steel lap joint. Scripta Mater 2012.
[3] Das H, Basak S, Das G, Pal TK. Influence of energy induced from processing parameters on the mechanical properties of friction stir welded lap joint of aluminum to coated steel sheet. Int J Adv Manuf Technol 2013;64:1653–61.
[4] Movahedi M, Kokabi AH, Seyed Reihani SM, Cheng WJ, Wang CJ. Effect of annealing treatment on joint strength of aluminum/steel friction stir lap weld. Mater Des 2013;44:487–92.
[5] Movahedi M, Kokabi A, Reihani S, Najafi H. Effect of tool travel and rotation speeds on weld zone defects and joint strength of aluminium steel lap joints made by friction stir welding. Sci Technol Weld Join 2012;17:162–7.
[6] Uematsu Y, Kakiuchi T, Tozaki Y, Kojin H. Comparative study of fatigue behaviour in dissimilar Al alloy/steel and Mg alloy/steel friction stir spot welds fabricated by scroll grooved tool without probe. Sci Technol Weld Join 2012;17:348–56.
[7] Thomas W. Friction stir butt welding. International Patent Application No. PCT/GB92/0220. 1991.
[8] Flores OV, Kennedy C, Murr L, Brown D, Pappu S, Nowak BM, et al. Microstructural issues in a friction-stir-welded aluminum alloy. Scripta Mater 1998;38:703–8.
[9] Uzun H, Dalle Donne C, Argagnotto A, Ghidini T, Gambaro C. Friction stir welding of dissimilar Al 6013-T4 To X5CrNi18-10 stainless steel. Mater Des 2005;26:41–6.
[10] Ghosh M, Kar A, Kumar K, Kailas S. Structural characterisation of reaction zone for friction stir welded aluminium–stainless steel joint. Mater Technol: Adv Perform Mater 2012;27:169–72.
[11] Tanaka T, Morishige T, Hirata T. Comprehensive analysis of joint strength for dissimilar friction stir welds of mild steel to aluminum alloys. Scripta Mater 2009;61:756–9.
[12] Lee W-B, Schmuecker M, Mercardo UA, Biallas G, Jung S-B. Interfacial reaction in steel–aluminum joints made by friction stir welding. Scripta Mater 2006;55:355–8.
[13] Chen CM, Kovacevic R. Joining of Al 6061 alloy to AISI 1018 steel by combined effects of fusion and solid state welding. Int J Machine Tools Manuf 2004;44:1205–14.
[14] Kovacevic R, Jiang WH. Feasibility study of friction stir welding of 6061-T6 aluminium alloy with AISI 1018 steel. J Eng Mnauf 2004;218:1323–31.
[15] Lee CY, Choi DH, Yeon YM, Jung SB. Dissimilar friction stir spot welding of low carbon steel and Al–Mg alloy by formation of IMCs. Sci Technol Weld Join 2009;14:216–20.
[16] Yılmaz M, Çöl M, Acet M. Interface properties of aluminum/steel friction-welded components. Mater Charact 2002;49:421–9.
[17] Bozzi S, Helbert-Etter A, Baudin T, Criqui B, Kerbiguet J. Intermetallic compounds in Al 6016/IF-steel friction stir spot welds. Mater Sci Eng, A 2010;527:4505–9.
[18] Chen T. Process parameters study on FSW joint of dissimilar metals for aluminum–steel. J Mater Sci 2009;44:2573–80.
[19] Kimapong K, Watanabe T. Effect of welding process parameters on mechanical property of FSW lap joint between aluminum alloy and steel. Mater Trans 2005;46:2211–7.
[20] Chen Y, Komazaki T, Tsumura T, Nakata K. Role of zinc coat in friction stir lap welding Al and zinc coated steel. Mater Sci Technol 2008;24:33–9.
[21] Chen YC, Komazaki T, Kim YG, Tsumura T, Nakata K. Interface microstructure study of friction stir lap joint of AC4C cast aluminum alloy and zinc-coated steel. Mater Chem Phys 2008;111:375–80.
[22] Watanabe T, Takayama H, Yanagisawa A. Joining of aluminum alloy to steel by friction stir welding. J Mater Process Technol 2006;178:342–9.
[23] Kuziak R, Kawalla R, Waengler S. Advanced high strength steels for automotive industry. Arch Civ Mech Eng 2008;8:103–17.
[24] Da Silva A, Aldanondo E, Alvarez P, Arruti E, Echeverria A. Friction stir spot welding of AA 1050 Al alloy and hot stamped boron steel (22MnB5). Sci Technol Weld Join 2010;15:682–7.
[25] Chung Y, Fujii H, Ueji R, Tsuji N. Friction stir welding of high carbon steel with excellent toughness and ductility. Scripta Mater 2010;63:223–6.
[26] Ikeda R, Matsushita M, Fujii H, Chung YD, Kitani Y, Ono M. Development of friction stir welding of high strength steel sheet. Sci Technol Weld Join 2011;16:181–7.
[27] Jafarzadegan M, Feng A, Abdollah-zadeh A, Saeid T, Shen J, Assadi H. Microstructural characterization in dissimilar friction stir welding between 304 stainless steel and st37 steel. Mater Charact 2012.
[28] Barnes S, Bhatti A, Steuwer A, Johnson R, Altenkirch J, Withers P. Friction stir welding in HSLA-65 steel: Part I. Influence of weld speed and tool material on microstructural development. Metall Mater Trans A 2012;43:2342–55.
[29] Ohashi R, Fujimoto M, Mironov S, Sato Y, Kokawa H. Effect of contamination on microstructure in friction stir spot welded DP590 steel. Sci Technol Weld Join 2009;14:221–7.
[30] Miles M, Pew J, Nelson T, Li M. Comparison of formability of friction stir welded and laser welded dual phase 590 steel sheets. Sci Technol Weld Join 2006;11:384–8.

[31] Miles M, Nelson T, Steel R, Olsen E, Gallagher M. Effect of friction stir welding conditions on properties and microstructures of high strength automotive steel. Sci Technol Weld Join 2009;14:228–32.
[32] Park SHC, Sato YS, Kokawa H, Okamoto K, Hirano S, Inagaki M. Boride formation induced by pcBN tool wear in friction-stir-welded stainless steels. Metall Mater Trans A 2009;40:625–36.
[33] Guerra M, Schmidt C, McClure JC, Murr LE, Nunes AC. Flow patterns during friction stir welding. Mater Charact 2002;49:95–101.
[34] Colligan K. Material flow behavior during friction welding of aluminum. Weld J 1999;75. p. 229s–37s.
[35] Reynolds AP. Visualisation of material flow in autogenous friction stir welds. Sci Technol Weld Join 2000;5:120–4.
[36] Coelho RS, Kostka A, dos Santos J, Pyzalla AR. EBSD technique visualization of material flow in aluminum to steel friction-stir dissimilar welding. Adv Eng Mater 2008;10:1127–33.
[37] Bouché K, Barbier F, Coulet A. Intermetallic compound layer growth between solid iron and molten aluminium. Mater Sci Eng, A 1998;249:167–75.
[38] Nandan R, DebRoy T, Bhadeshia HKDH. Recent advances in friction-stir welding – process, weldment structure and properties. Prog Mater Sci 2008;53:980–1023.
[39] Rathod M, Kutsuna M. Joining of aluminum alloy 5052 and low-carbon steel by laser roll welding. Weld J N Y 2004;83:16.
[40] Kobayashi S, Yakou T. Control of intermetallic compound layers at interface between steel and aluminum by diffusion-treatment. Mater Sci Eng, A 2002;338:44–53.
[41] Bouayad A, Gerometta C, Belkebir A, Ambari A. Kinetic interactions between solid iron and molten aluminium. Mater Sci Eng, A 2003;363:53–61.
[42] Yeremenko V, Natanzon YV, Dybkov VI. The effect of dissolution on the growth of the Fe2Al5 interlayer in the solid iron–liquid aluminium system. J Mater Sci 1981;16:1748–56.
[43] Shahverdi HR, Ghomashchi MR, Shabestari S, Hejazi J. Microstructural analysis of interfacial reaction between molten aluminium and solid iron. J Mater Process Technol 2002;124:345–52.
[44] Sundman B, Ohnuma I, Dupin N, Kattner UR, Fries SG. An assessment of the entire Al–Fe system including D03 ordering. Acta Mater 2009;57:2896–908.
[45] Tylecote RF. The solid phase welding of metals: Edward Arnold; 1968.
[46] Johnson M, Mikkola D, March P, Wright R. The resistance of nickel and iron aluminides to cavitation erosion and abrasive wear. Wear 1990;140:279–89.
[47] Knibloe J, Wright R, Trybus C, Sikka V. Microstructure and mechanical properties of Fe3Al alloys with chromium. J Mater Sci 1993;28:2040–8.